HiLL PUBLISHING

Journal of Applied Mathematics and Computation, 2024, 8(1), 50-58
https://www.hillpublisher.com/journals/JAMC/
ISSN Online: 2576-0653
ISSN Print: 2576-0645

Acceleration of the Iterative Procedure for Correction of Optoacoustic Images

Alexandr G. Rudnitskii

Institute of Hydromechanics, National Academy of Sciences of Ukraine, Kyiv, Ukraine.

How to cite this paper: Alexandr G. Rudnitskii. (2024) Acceleration of the Iterative Procedure for Correction of Optoacoustic Images. *Journal of Applied Mathematics and Computation*, 8(1), 50-58.
DOI: 10.26855/jamc.2024.03.006

Received: February 28, 2024
Accepted: March 27, 2024
Published: April 26, 2024

***Corresponding author:** Alexandr G. Rudnitskii, Institute of Hydromechanics, National Academy of Sciences of Ukraine, Kyiv, Ukraine.

Abstract

The main goal of the work was to further improve the efficiency of a numerical algorithm designed to correct artifacts and distortions that arise during image restoration in optical-acoustic tomography problems. The proposed iterative scheme for improving biomedical optoacoustic images is based on Banach's fixed point theorem. The challenge was to determine the fastest and most efficient acceleration method applicable to the developed algorithm. In a numerical optical-acoustic experiment, a biological environment with a reconstructed object built into it was simulated. The simulations were run for two-dimensional and three-dimensional numerical models to study the effectiveness of the proposed algorithms. The quality of the reconstruction was determined by both quantitative and visual assessments of the results obtained. The convergence of different acceleration methods and the quality of the output images were analyzed in terms of PSNR (peak signal-to-noise ratio) and SSIM (structure similarity index).

Keywords

Optoacoustic images, numerical simulation, accelerated gradient descent, fixed-point iteration acceleration

1. Introduction

Optoacoustics is a hybrid imaging technique that combines the strengths of both optical and acoustic imaging. This method relies on the absorption of pulsed light by tissue inhomogeneities, which causes their rapid and localized thermoelastic expansion and creates an acoustic wave. The acoustic wave can then be detected by ultrasonic transducers and used to create images of biological structures, including those hidden under other tissues.

Optoacoustic (OA) imaging has a crowning place within other imaging techniques because it has a number of advantages over traditional imaging modalities such as X-ray, CT, and MRI. It is non-invasive and does not involve ionizing radiation. One of the key advantages of optoacoustic imaging is its ability to provide high-resolution images of biological tissues at depths of several centimeters. This is because the acoustic waves generated by light can penetrate deep into tissues, allowing visualization of internal organs. This makes it possible to use OA imaging both in clinical settings and in preclinical studies. It can be used to study the heart, brain, and other organs, and to investigate the effects of treatments on targeted organs *in vivo*.

In practice, pressure waves originating from biological absorbers are rather weak, so the creation of a high-quality and reliable reconstruction of OA images is difficult due to the inevitable presence of measurement noise in the obtained data. In addition, distortions and artifacts in the reconstructed image can be associated with the features of a particular reconstruction algorithm. Therefore, the problem of eliminating distortions in reconstructed OA images is very relevant for the effective use of this method in clinical practice and scientific research [1].

The main goal of the work was to develop and study the fastest possible numerical algorithm designed to correct artifacts and distortions caused by the peculiarities of the image restoration method in optical-acoustic tomography problems. The

motivation for this work is to further improve the efficiency of the method proposed in [2]. The focus of the research is to investigate the application of fixed-point iteration acceleration techniques and gradient descent methods. The task is to determine the most efficient acceleration method in terms of its performance.

The organization of work is as follows. In Section 1, we present a brief introduction to the direct and inverse problems of optoacoustics, as well as a proposed iterative algorithm for correcting reconstructed OA images. Section 2 describes in more detail the acceleration methods of our iterative approach, the numerical experiments, and the results of modeling the reconstruction of OA images for the 2D and 3D cases. The Conclusion presents the results and prospects of the developed algorithm.

2. Iterative optoacoustic reconsruction algorithm

The process of solving the direct problem of optoacoustics is to find the pressure field of the sound wave $p(\mathbf{r},t)$ by the known distribution of heat sources $H(\mathbf{r},t)$ (here $\mathbf{r}$ – the spatial coordinate of the points, t – time). For definiteness, we assume that sound sources arise as a result of laser illumination of the environment. This spatiotemporal dependence $p(\mathbf{r},t)$ created by the heat source $H(\mathbf{r},t)$ in an acoustically homogeneous infinite medium can be obtained from the equation [3]:

$$\left[\nabla^2 - \frac{1}{c^2}\frac{\partial^2}{\partial t^2}\right] p(\mathbf{r},t) = -\frac{\beta}{c_p}\frac{\partial}{\partial t} H(\mathbf{r},t), \tag{1}$$

where c is the ultrasound velocity, β – is the isobaric expansion coefficient, and c_p *is* the specific heat capacity at constant pressure (here effects of viscosity and thermal conductivity are ignored).

The heat-source term $H(\mathbf{r},t)$ is nonzero only during a short laser pulse. Therefore, the heart source may be presented as the product of the spatial distribution of the absorbed energy and the time dependence of laser intensity: $H(\mathbf{r},t) = Q(\mathbf{r})\cdot\delta(t)$. Here $\delta(t)$ is the Dirac delta function. The initial acoustic pressure arising due to the absorption of pulsed radiation by optical inhomogeneities at time $t = 0$ is defined as $p_0(\mathbf{r}) = \Gamma\cdot Q(\mathbf{r})$, where $\Gamma = c^2\beta/c_p$ is the dimensionless and temperature-dependent Grüneisen parameter, which characterizes the efficiency of the OA transformation of absorbed light into acoustic pressure. Under these assumptions, the distribution of the pressure field at the point $\mathbf{r}$ and at any time t can be expressed as [3]

$$p(\mathbf{r},t) = \frac{1}{2\pi c^2}\int_{V'} \frac{\frac{\partial}{\partial t}\left(p_0(\mathbf{r}')\delta(t - |\mathbf{r}-\mathbf{r}'|/c)\right)}{|\mathbf{r}-\mathbf{r}'|} dV', \tag{2}$$

where V' is the volume containing the distributed OA sources.

The inverse problem of optoacoustics is to restore absorbing structures inside the irradiated body, i.e. it is necessary to determine the initial acoustic pressure $p_0(\mathbf{r},t = 0) = p_0(\mathbf{r})$ from the pressure signals $p_s(\mathbf{r},t)$ received on the surface S of the volume V' [4].

There are a number of methods for restoring the distribution of sources in a medium: the delay and sum algorithm, the back-projection method, and the Fourier reconstruction algorithm [5, 6].

Each of these methods has its own advantages and limitations, and each is based on its own specific mathematical model. In real situations, the model's assumptions are only partially met, which leads to distortions in the reconstructed images. The specifics of these distortions are different when using different reconstruction methods, different locations of receivers, and different geometry of the reconstructed object.

To overcome the strong dependence of image quality on these factors we proposed a method for reducing distortions in reconstructed OA images [2]. It is based on the Banach fixed point theorem [7]. This theorem guarantees the existence and uniqueness of a fixed point for some mappings of metric spaces. It also contains a constructive method for finding this point. The theorem is named after Stefan Banach, a Polish mathematician who established it in 1922.

Theorem (***Banach Fixed Point Theorem***)

Let $(\mathbb{Q},\rho)$ *be a non-empty complete metric space with a contraction mapping* F: $\mathbb{Q} \to \mathbb{Q}$, i.e., $\exists\alpha\in[0,1)$: $\rho(F(x), F(y))\le\alpha\rho(x,y)$, $\forall x,y \in \mathbb{Q}$.

Then the following conclusions hold:

- F *has a unique fixed point* $x^*\in\mathbb{Q}$, i.e. $F(x^*) = x^*$;
- for any $x_0\in\mathbb{Q}$ the sequence $x_{n+1} = F(x_n)$ converges to x^* for $(x_n)_{n\in\mathbb{N}}$, $n \ge 1$.

Let X is an unknown input image, Y is the reconstructed (given) image, and $F(\cdot)$ is a mapping (operator) that transforms ithe nput image into a reconstructed image (image with distortions and artifacts) (Fig. 1):

$Y = F(X)$, $X,Y \in \mathbb{R}^d$.

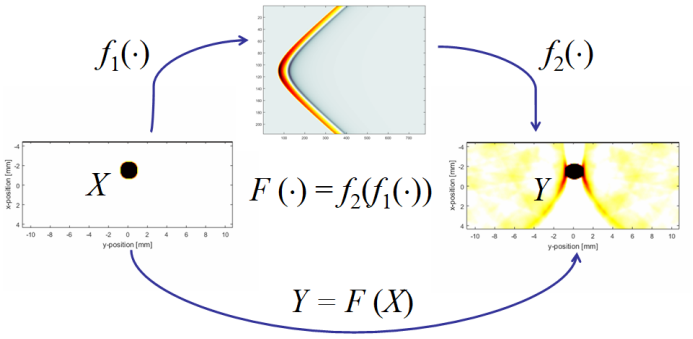

Figure 1. Scheme of OA reconstruction.

The problem statement is the following: for a given $F(X^*)$, make an estimate of X^*. In our case, the operator F can be represented as the result of alternately applying the functions $f_1(\cdot)$ and $f_2(\cdot)$: $F(\cdot)= f_2(f_1(\cdot))$, where $f_1(\cdot)$ is the operator that performs the direct problem of optoacoustics (equation (2)), and $f_2(\cdot)$ is the operator that specifies solution of the inverse problem.

There is a direct and obvious way to solve this problem: find the inverse function $F^{-1}(X)$. Then $X= F^{-1}(F(X))$. To do this, it is necessary to have an explicit description of $F(\cdot)$. In our particular situation, we have access to the operator $F(\cdot)$, and this operator we can apply to a given image X any number of times and observe the output. However, we may not have an explicit description of $F(\cdot)$. For example, we may not have explicit code for solving the forward optoacoustics problem $f_1(\cdot)$, the algorithm for the inverse problem $f_2(\cdot)$, or both operators together. Therefore we can only calculate $F(\cdot)$ in the forward direction for the known physical model we have adopted. However, it is possible to obtain a refined solution of the inverse problem of optoacoustics by forming a sequence of images $\{I_q\}$ $(q \geq 1)$ such that $I_q = F(I_{q-1})$ using the Banach fixed point theorem. Here $F(\cdot)$ transforms the initial acoustic pressure arising due to absorption by optical inhomogeneities $p_0(\mathbf{r})$ to its zero approximation $p_0^{(0)}(\mathbf{r}) = I_0$ (see Fig.1).

In [2], we used this approach to improve the quality of reconstructed OA images. The drawback is that sometimes such an iterative process requires too many iterations to get the desired quality. As a result, processing speed may be unacceptably slow. In the work [2], two iterative schemes were used to enhance reconstructed images: the approach corresponding to the Picard method [8] and the gradient descent scheme proposed by Steffensen [9]. In this article, we propose to use acceleration methods to solve the problem of improving reconstructed OA images. To the best of our knowledge, it has not been found in the literature for this particular problem.

3. Acceleration algorithms

3.1 Fixed-point iteration acceleration

There are several iterative methods based on the Banach's fixed point theorem. Following the work of [10], let's designate their T-method, TDA-method (total derivative approximation), and p-method.

Iterative scheme for the T-method:

$$X_{q+1} = X_q + H_q;\ H_q = Y - F(X_q);\ X_0 = Y; \tag{3}$$

scheme for the TDA-method:

$$X_{q+1} = X_q + \alpha[F(X_q + H_q) - F(X_q)]; \tag{4}$$

and for p-method:

$$X_{q+1} = X_q + [F(X_q + H_q) - F(X_{q-1} H_q)]/2. \tag{5}$$

Different fixed-point acceleration methods can be applied to each of these iterative schemes: Anderson, Chebyshev, Irons and Wynn approaches.

Anderson Acceleration (AA) is a technique for improving the convergence of fixed-point iterations [11]. The general idea of the Anderson acceleration method is that we first perform a fixed-point iteration, as in one of the equations (3-5). The minimization problem is then used to improve the iteration. Thus, to generate a new estimate, not just the last iteration is used, but also several previous ones:

$$x_{k+1} = F(x_k) - \sum_{j=1}^{m-1} \theta_j^k \left(F(x_{k-m+j+1}) - F(x_{k-m+j}) \right),$$

$$\min_{\theta} \left\| G(x_k) - \sum_{j=1}^{m-1} \theta_j^k \left(G(x_{k-m+j+1}) - G(x_{k-m+j}) \right) \right\|_2^2, \quad (6)$$

where $G(x) = F(x) - x$ and m is the number of past iterations.

It is important to note that the implementation of the algorithm does not require the calculation of derivatives. As in [10], we used AA with depth m=2, i.e. only for two optimization parameters θ_0 and θ_1, which were calculated according to the method proposed in [12]. Details of other testing methods can be found in [13]. We do not present them here, since in our numerical experiments it was AA that turned out to be the most promising method for accelerating the iterative process.

3.2 Accelerated gradient descent

The gradient descent method is a numerical method for finding the local minimum/maximum of a function by moving along a gradient. This was first proposed by Augustin-Louis Cauchy in 1847 [14]. The gradient descent algorithm finds parameters to minimize the objective function (differences between actual and predicted results). The algorithm allows to iteratively calculate the next point on the path to the minimum of the objective function $C(X)$, using the gradient (or approximate gradient) of its current position:

$$X_{q+1} = X_q - \lambda \nabla C(X_q).$$

The parameter λ scales the gradient and controls the step size.

There is a number of accelerated gradient descent (AGD) schems to reduce the number of iterations and overcome some of disadvantages of this method [15]. In [16], it was proved that T-, TDA- and p-methods can be considered as gradient descent algorithms, so AGD methods can be used to improve their performance. In this article, we only study the MGD (momentum method), NAG (Nesterov method), and Adam methods.

Momentum-based gradient descet (MGD). This method is based on taking into account information about previous weights. The parameter update is based not only on the current gradient but also on the moving average of past gradients.

$$X_{q+1} = X_q + V_q;$$
$$V_q = \gamma V_{q-1} - \lambda \nabla C(X_q + V_{q-1}).$$
$$\nabla C = (Y - F(X_q)).$$

Accelerated Nesterov Gradient (NAG): Instead of estimating the gradient at the current position, the method first estimates the gradient at the additional predictor term based on the current momentum vector.

$$X_{q+1} = X_q + V_q;$$
$$V_q = \gamma V_{q-1} - \lambda \nabla C(X_q + \gamma V_{q-1}).$$
$$\nabla C = (Y - F(X_q)).$$

Adam: This method adaptively estimates moments. It tracks two exponentially decreasing averages: an exponentially decreasing average of past gradients and an exponentially decreasing average of past squared gradients.

More details can be found in [16].

3.3 Quality metrics

In our simulation, we assume that the original image is known. Therefore, as criteria for evaluating the quality of the output image, it is advisable to use such quality metrics as the peak signal-to-noise ratio (PSNR) and the structural similarity index (SSIM). The first one (PNSR) measures the absolute errors in each pixel, and the second one (SSIM) evaluates the image quality based on structural information. Higher PSNR values indicate better reconstruction quality. This measure of quality is still widely used to assess the quality of reconstruction, for example [17], despite the fact that PSNR does not always match the human perception of image quality [18].

SSIM values range from –1 to 1, where 1 corresponds to an accurate reconstruction, 0 indicates no similarity, and –1 indicates perfect anti-correlation. This index takes into account image parameters such as luminance, contrast, and structure. These parameters are evaluated, respectively, through the intensities, standard deviations, and covariances of the compared images in each pixel. After avaraging we have one single quality measure of the entire image [19].

In order to evaluate and compare the performance of each acceleration method, we conducted numerical experiments to

calculate these metrics (PSNR and SSIM) as functions of the number of iterations.

4. Testing

In order to numerically assess the quality of photoacoustic reconstruction of 2D and 3D images *in silico* (based on modeling) and solve the problem of propagation of acoustic waves in biological tissue, the *k*-Wave software package was used - a set of tools in the MATLAB environment. Its use allows modeling systems with acoustic sources and receivers of various shapes and sizes. The numerical model is based on the transition to *k*-space. Spatial gradients are computed here using a Fast Fourier Transform scheme. When calculating temporal gradients, an adjusted *k*-spatial difference scheme is used [20].

Our correction algorithm was tested numerically using phantoms simulating tissue containing inclusions with a higher absorbance than the background. An environment that was close in its parameters to biological tissues was modeled: a homogeneous medium with a density $\rho_0 = 1020$ kg/m^3 and sound speed $c_0 = 1510$ m/s. To showcase the influence of various acceleration methods on quality measures, 2D and 3D numerical phantoms (optical-acoustic reconstruction objects) were built. For the two-dimensional space, a circular disk and a two-dimensional model of the vascular tree were chosen as numerical phantoms, while for the 3D space, a three-dimensional model of the aorta with an aneurysm was used. The two-dimensional blood vessel-like model is concluded in the *k*-Wave software package. The physical size of the sample for 2D detection is 4.6×4.6 mm and 10.3×10.3×5.3 mm for 3D detection. In the 2D case, the sensors were located linearly on the upper face of the rectangular sample; in 3D space, the sensors were distributed over the upper surface of the parallelepiped. For the reconstruction of the given objects, the back projection algorithm with the Fourier transform was used.

The PSNR and SSIM values for each specific AFP and AGD method were calculated per iteration. The results obtained during the reconstruction of the circular disk and the two-dimensional vascular tree are shown in Fig. 2 and Fig. 3, respectively. For visualization convenience, the curves for the T-method (without acceleration) are plotted with a black curve with circular markers.

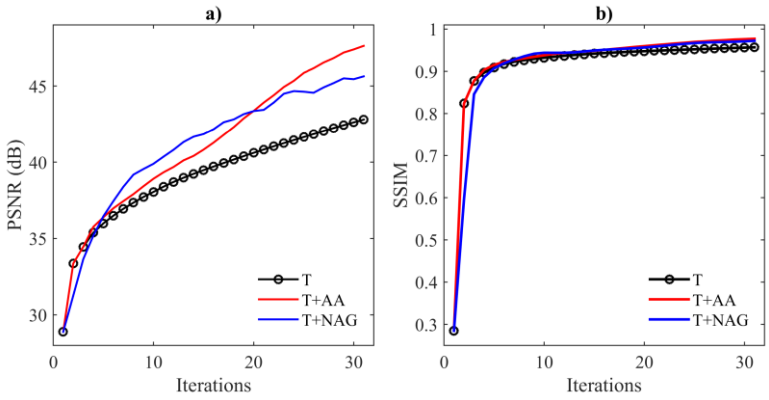

Figure 2. Comparison of Anderson acceleration and Nesterov acceleration (λ=0.77, γ=0.5) for the T-method in the reconstruction of a circular disk.

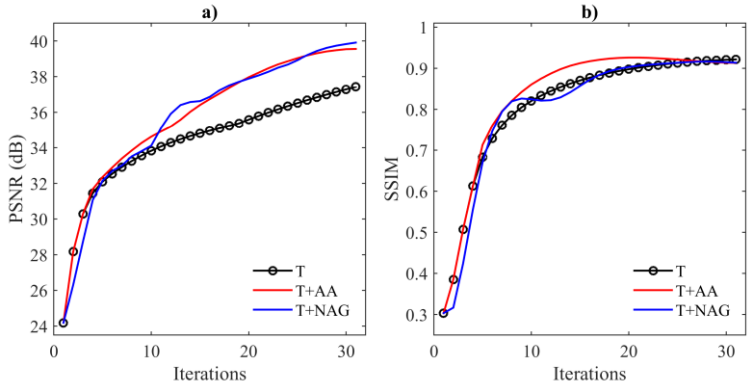

Figure 3. Comparison of Anderson acceleration and Nesterov acceleration (λ=0.77, γ=0.5) for the T-method in the reconstruction of a 2D vascular tree.

We see that the use of acceleration significantly improves the results obtained with the same number of iterations. For example, for a circular disc, applying our method with 30 iterations increases the PSNR from 28 to 43.15 dB for the T-method, to 48 dB for the AA method, and to 46 dB for the NAG method.

The implementation of the AA and Nesterov methods does not require the calculation of derivatives and norms, and the original function is called only once. This is ideal for speeding up the correction method. From both Fig.2 and Fig.3 it can be seen that for the objects selected for reconstruction (disc and vessel tree), the quality of recovery by acceleration methods is achieved in a much smaller number of iterations than for the original T-method. Both algorithms require about half as many iterations, both in terms of PSNR and SSIM.

The Anderson acceleration method does not require parameter settings. The only parameters that are set in advance are the number of iterations and the number of optimization parameters (in our case, m=2). At the same time, the efficiency of image restoration by the Nesterov method significantly depends on the settings. Sometimes, with poorly chosen parameters λ and γ (see eq(3,4)), the efficiency of quality restoration may be lower than that of the T-method (with the same number of iterations).

In addition, Fig. 2 and Fig. 3 show that although with a successful choice of parameters λ and γ iterations with Nesterov acceleration and Anderson acceleration converge almost equally, Nesterov's method may demonstrate some instability.

To visually illustrate the difference in the quality of image restoration, Fig. 4 shows the original image and its reconstructed versions. The OA source $p_0(x,y)$ here is the round disk shown in Fig. 4a), and the result of its reconstruction, implemented using the *k*-Wave algorithm, is shown in Fig. 4b). We see that the intensity of the reconstructed image $p_0^{(0)}$ is lower than that of the original sample (~20%), and its edges are smoothed. In addition, artifacts in the form of spots and arcs appeared on an initially clean background. Fig. 4c) shows the image improved by the AA method after the 30-th iteration. It is obvious that the distortions noticeable at the 0-th iteration (Fig. 4b) have been successfully removed by the corrective algorithm.

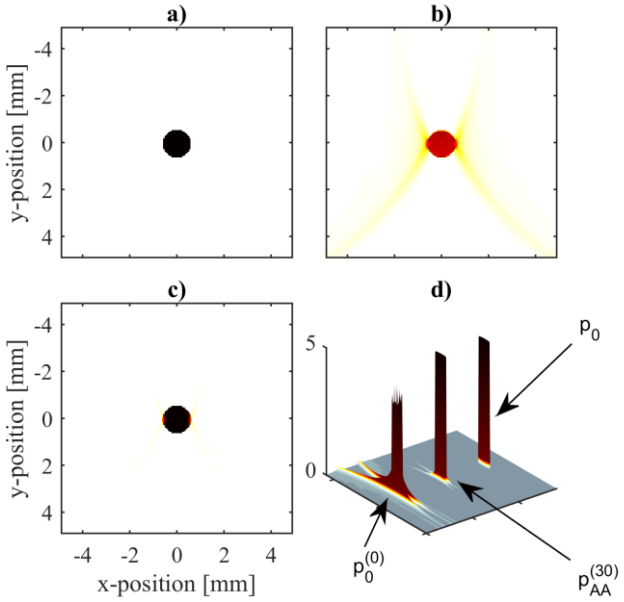

Figure 4. Comparison of Anderson acceleration and *k*-Wave reconstruction in the reconstruction of a 2D disk: a) original source $p_0(x,y)$; b) *k*-Wave reconstruction $p_0^{(0)}$; c) AA method $p_{AA}^{(30)}$; d) 3d comparison.

Figure 4d) shows these results in 3D (along the applicate axis the source intensity is plotted). Here in the foreground is the result of the *k*-Wave reconstruction $p_0^{(0)}$ (the first "tower"), in the middle is the 30-th iteration of the AA method $p_{AA}^{(30)}$, and in the background is the last object - the source $p_0(x,y)$.

More details can be seen in Fig.5., where the central linear sections of the original object $p_0(x,y)$ and its reconstructions are shown. A two-dimensional zero-approximation image of the reconstructed circular disk $p_0^{(0)}$ is shown in Fig. 5a) and arrows mark its vertical and horizontal sections. The corresponding linear profiles of the original object and its reconstructions are shown in Fig. 5b) and Fig. 5c).

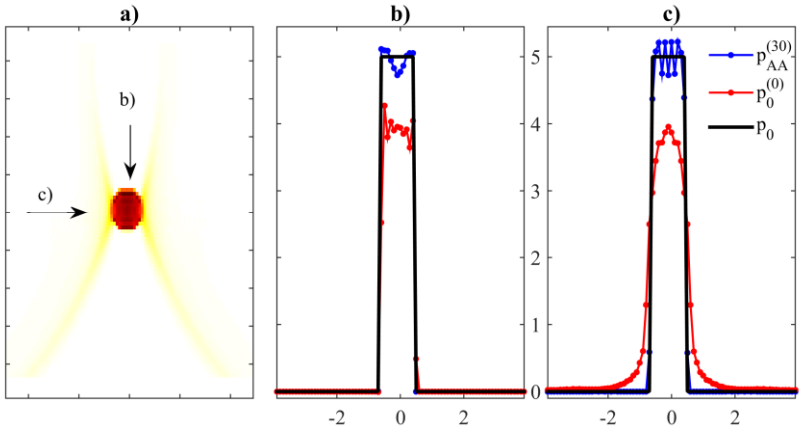

Figure 5. a) Zero iteration of the disk image $p_0^{(0)}$; b) and c) linear profiles of AA-reconstructed image $p_{AA}^{(30)}$ and original image p_0.

It can be seen that the errors and reconstruction artifacts present in the zero approximation have been successfully eliminated: the edges of the corrected image become sharper, and its intensity is almost the same as the original one. Similar results were obtained for more complex objects - two-dimensional vascular tree phantom and three-dimensional model of an aorta with an aneurysm.

A feature of the reconstructed image of a two-dimensional vascular tree model is that the quality of reconstruction of horizontal and vertical linear structures differs significantly (see Fig. 6b). This is due to limited visibility and the linear arrangement of the sensors only on the upper face of the rectangular sample. Figure 6c) demonstrates that in this case, too, the proposed approach can significantly improve the quality of the reconstructed image.

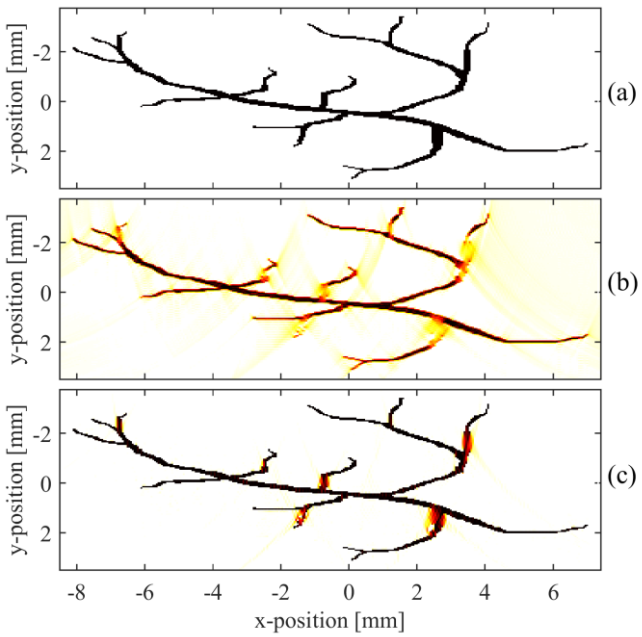

Figure 6. Comparison of Anderson acceleration and *k*-Wave reconstruction in the reconstruction of a 2D vascular tree: a) original image; b) *k*-Wave reconstruction $p_0^{(0)}$; c) AA-reconstructed image $p_{AA}^{(30)}$.

A similar observation can be made when applying the AA method to a 3D numerical phantom of an aorta with an aneurysm (Fig. 7). We see that the quality of the reconstructed object is significantly better: the intensity, edges and boundaries of the vascular branches are reproduced much more accurately. There is almost no noticeable difference between the original and enhansed images.

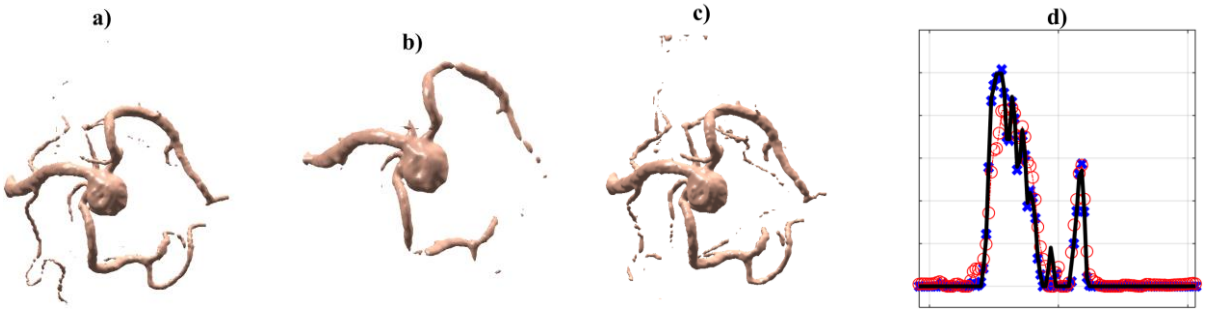

Figure 7. Reconstruction of a 3D phantom of the aorta with an aneurysm: a) original image; b) reconstructed image; c) corrected image; d) linear profiles of images in the central x-z section of the 3D phantom.

At the conclusion of this section Fig. 8 shows the results of applying the proposed acceleration methods to TDA and p-methods. As shown in this figure, the proposed acceleration approaches are ineffective when dealing with TDA and p-methods. We see that their accelerated versions do not provide improvements in PSNR and SSIM. Thus, we can conclude that for our reconstruction problem (for the physical-mathematical model we adopted), the T-method and its accelerated versions are algorithms that can achieve a higher level of improvement compared to TDA and p-based algorithms. And for the T-method, the best choice is the AA acceleration method.

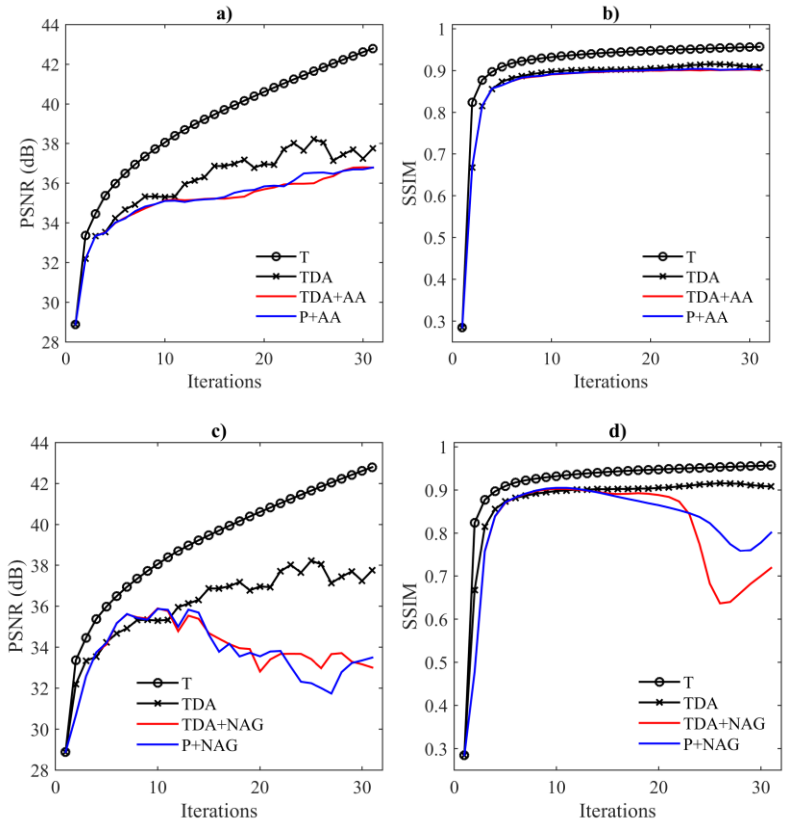

Figure 8. Comparison of Anderson acceleration and GD acceleration for the TDA-method in the reconstruction of a circular disk.

5. Conclusion

In this paper, we examined an algorithm designed to correct artifacts and distortions in OA images associated with model assumptions and limitations, and proposed the use of acceleration schemes for it. We have successfully demonstrated that the use of the proposed methods accelerates the iterative process of improving the quality of optoacoustic images. It is shown that acceleration methods, such as the Anderson method and the Nesterov method, applied to the T-method,

significantly improve the performance of the algorithm when restoring various 2D and 3D images.

However, not all acceleration methods achieve their goal equally successfully. The AA method combines well with the T-method and does not require additional configuration. Nesterov's method also significantly speeds up the achievement of the desired quality, but requires preliminary fine-tuning of two parameters, which may take some time. At the same time, the application of these acceleration methods (AA and NAG) to the TDA method and the p-method is inferior to the T-method and can even worsen the quality of the original images.

References

[1] M. Sandbichler, F. Krahmer, T. Berer, P. Burgholzer, and M. Haltmeier. (2015). A Novel Compressed Sensing Scheme for Photoacoustic Tomography SIAM J. Appl. Math., 75 (6), 2475-2494.

[2] A. G. Rudnitskii. (2022) Iterative Image Correction Scheme for Optoacoustic Tomography. Acoustical Physics, 68, N4, pp.395-402.

[3] V. E. Gusev and A. A. Karabutov. Laser Optical Acoustics (Nauka, Moscow, 1991) [in Russian].

[4] T. D. Khokhlova, I. M. Pelivanov, and A. A. Karabutov. (2009). Methods of optoacoustic diagnostics of biological tissues Acoust. Phys., 55, 674-684.

[5] Rosenthal A., Ntziachristos V., Razansky D. (2013). Acoustic inversion in optoacoustic tomography: A review. // Current medical imaging reviews, 9. No. 4, 318-336.

[6] Kuchment P, Kunyansky L. (2009). Mathematics of photoacoustic and thermoacoustic tomography. Handbook of Mathematical Methods in Imaging Springer, 819-861.

[7] Banach, Stefan (1922). Sur les opérations dans les ensembles abstraits et leur application aux équations intégrales. Fundamenta Mathematicae, 3: 133-181. doi:10.4064/fm-3-1-133-181.

[8] V. Berinde. (2007). Iterative Approximation of Fixed Points (Springer, 2007).

[9] Steffensen, I.F. (1933). Remarks on Iteration. Scandinavian Actuarial Journal, 1933, 64-72. https://doi.org/10.1080/03461238.1933.10419209.

[10] Guang Deng, Fernando Galetto. Fast iterative reverse filters using fixed-point acceleration. Signal, Image and Video Processing. https://doi.org/10.1007/s11760-023-02584-1.

[11] D. G. Anderson. (1965). Iterative procedures for nonlinear integral equations. Journal of the ACM (JACM), 12, N. 4 . 547-560.

[12] https://ctk.math.ncsu.edu/TALKS/Anderson. pdf.

[13] F. J. Galetto, G. Deng, (2022). Fast image reverse filters through fixed point and gradient descent acceleration. arXiv:2206.10124v1 [eess.IV] 21 Jun 2022.

[14] Claude Lemarechal. (2012). Cauchy and the Gradient Method Doc. Math. Extra., 251-254.

[15] M. J. Kochenderfer, T. A. Wheeler. (2019). Optimization algorithms. MIT Press.

[16] F. J. Galetto, G. Deng. (2021). Reverse image filtering using total derivative approximation and accelerated gradient descent. arXiv preprint arXiv: 2112.04121, 2021.

[17] S. M. Spann, K. S. Kazimierski, C. S. Aigner, M. Kraiger, K. Bredies, and R. Stollberger. (2017). Spatio-temporal TGV denoising for ASL perfusion imaging. NeuroImage, 2017. Aug 15:157:81-96. doi: 10.1016/j.neuroimage.2017.05.054. Epub 2017 May 27.

[18] Z. Wang, A. C. Bovik. (2009). Mean squared error: Love it or leave it? a new look at signal fidelity measures. IEEE Signal Processing Magazine, 26(1):98-117.

[19] Wang Zhou, Bovik, Alan C., Sheikh, Hamid R., Simoncelli, Eero P. (2004). Image Quality Assessment: From Error Visibility to Structural Similarity. IEEE Transactions on Image Processing, 2004.Vol. 13, No. 4, pp. 600-612.

[20] B. E. Treeby. (2013). IEEE Trans. Ultrason., Ferroelectr., Freq. Control, No. 10, 2208.